communications materials

Review article

https://doi.org/10.1038/s43246-024-00568-3

Solid-state inorganic electrolytes for next generation potassium batteries

Check for updates

Jonas Grill[1], Simon K. Steensen[2], Diana Lucia Quintero Castro[3], Ivano E. Castelli[2] & Jelena Popovic-Neuber[1]

Necessary diversification of battery chemistry and related cell design call for investigation of more exotic materials and configurations, such as solid-state potassium batteries. In the core of their development lies the necessity of discovering new and electrochemically more efficient inorganic solid-state electrolytes. This review focuses on suitable chemical structures, their fundamental properties and status of the materials synthesis, related electrochemical performance, contemporary characterization techniques and modeling efforts for inorganic solid-state potassium electrolytes.

Solid-state batteries (SSB) have been in the focus of the academic scientific community and companies dealing with battery technology, related materials, and their electrochemistry due to promise of higher energy and power density, higher device safety and stability, as well as potentially fast charging capabilities[1–5]. The key challenges for development of SSB technologies are (i) design of solid-state electrolytes (SSEs) requiring a minimum stack pressure (few MPa) for long term operation, (ii) development of stable high-rate and high-capacity anodes such as alkali metals and silicon, (iii) design of low-cost SSEs with high ionic conductivities in thick and optimized cathodes, (iv) optimization of SSE interfaces, (v) sustainability improvement[6–8]. Thus, development of SSEs and related interfaces lies in the core of the current efforts. Ragone plots comparing specific energy and power of different materials suggest that much is to be done to improve room temperature performance of cells with inorganic SSEs, while the cells containing inorganic/polymer composite SSEs behave well at elevated temperatures (50–100 °C), at least in the lithium case[1].

To achieve the necessary energy densities, the issues related to the reactivity of K anode resulting in continuous solid electrolyte interphase (SEI), dendrite, and porous and 'dead' electrode growth need to be solved[9]. Regarding the SEI improvement, in the case of K metal, Pilling-Bedworth ratios (Supplementary Information, Table S1) suggest that only $KHCO_3$ as well as some polysulfides and pyrosulfates (K_2S, K_2S_5 and $K_2S_2O_7$) may form a stable non-porous artificial SEI layer. One of the approaches to circumvent the "dead" metal formation is the so-called anode-free or anodeless SSB, where the alkali metal is electrodeposited at the beginning of operation[10–12]. However, the SEI evolution is expected to be even more amplified in this case, since freshly deposited alkali metals are expected to be more reactive as they are not covered by native films. Another option for improving the energy density is employment of a silicon anode[13]. Even though it is expected that potassium may react with silicon, it has been shown that the reactions occur at either high temperature (above 550 °C) or high pressure (4 GPa)[14]. On the other hand, theoretical calculations suggest high K^+ diffusion in amorphous Si due to weak electrostatic K-single bond-Si attraction, high carrier ion concentration, and the formation of isolated Si_n ($n = 3–5$) clusters during the potassiation process[15]. In addition to all previously mentioned possibilities, new solid-state electrolytes offering high ionic conductivity should be developed, with sulfides, halides, polymers and oxides being at the forefront[16]. Ionic conductivity of SSEs should be high and even higher than in the liquid electrolyte case (ca. 10 mS cm^{-1}), since they are, in most configurations, mixed with cathode materials[8]. Often, it is pointed out that SSBs should offer higher materials stability compared to cells containing liquid electrolyte since the electrode cross-talk is circumvented[17]. Non-uniform alkali metal flux is however a fingerprint of such cross-talk and should not be neglected in real systems[18]. Electrochemical high-throughput screenings of crystal structures have been generally employed in recent years to accelerate material search for structures with desired properties within battery research. Utilizing availability of computational resources allows for integration of ab-initio methods, geometrical characteristics structures, machine learning and other techniques used for screenings of electrode and solid electrolyte materials by filtering the key aspects such as electrochemical stability, activation barriers, volume expansion and open-circuit-voltage insight in the case of electrodes throughout the process[19–24].

In terms of technological feasibility, lithium-based SSBs seem to be techno-economically comparable with the commercial lithium-ion technology[25]. Sodium and potassium ion batteries show comparable environmental performances and lower supply risks[26]. The techno-economical predictions of K-SSBs are difficult, as high uncertainties are expected in terms of solid state electrolyte price, K metal price and required metal excess[27]. In general, SSBs are slightly more expensive than conventional liquid-electrolyte based batteries due to higher price of manufacturing and processing of solid-state electrolytes, as well as full cells, and are still far

[1]Department of Energy and Petroleum Engineering, University of Stavanger, Stavanger, Norway. [2]Department of Energy Conversion and Storage, Technical University of Denmark, Kongens, Lyngby, Denmark. [3]Department of Mathematics and Physics, University of Stavanger, Stavanger, Norway.
e-mail: jelena.popovic-neuber@uis.no

away from necessary 100 $ kWh^{-1} [28]. For example, densification is very important for all components of SSBs, which results in potentially different production conditions necessary[29]. Also, the difference in pressure needed for successful operation is still considerable (1 vs. several MPa)[30]. Recently, it has been shown that it is not sufficient to focus solely on increasing materials supply or on enhancing cell capacity of SSB, since these two parameters are coupled[31]. Another problem in terms of commercialization of SSBs is their scalability, where high throughput processes might be beneficial but are challenging for already existing battery industry[32]. From a production point of view, additional processes involving compaction of materials through isostatic pressing are necessary[33]. In terms of design, bipolar design is seen as a potentially successful technique for improvement[34].

In the first part of this review, we give insight into bulk performance parameters, promising chemical structures and related ion transport mechanisms in currently known inorganic K-conductors of interest as SSEs. Secondly, we focus on the efforts to understand and solve the issues related to the anode (predominantly K metal)/K SSE interphase instability. For more information on cathode/SSE interface, we suggest consulting refs. 6,7. Finally, we give a contemporary overview of characterization techniques targeting structural and morphological evolution on several scales, as well as electrochemical and *operando*/in situ techniques.

Bulk performance parameters, chemical structures, and ion transport mechanisms

Key parameters governing the electrochemical performance of SSEs include high room temperature ionic conductivity linked with very low electronic conductivity (e.g., electronic transference number, $t_{el,}$ close to zero), low activation energy for ion transport, E_A, and high alkali metal diffusion coefficient, D_K. The complexity of the bulk performance is amplified by the fact that migration of ions in SSB is a multiscale process, encompassing both atomic and device scale[35]. The macroscopic diffusivity and its Arrhenius expression is obtained from the barrier of the single diffusion event by transition state theory, while on the macroscopic scale, the diffusion coefficient can be described by Fick's laws[36]. Favorable migration pathways are a function of availability and interconnectivity of different sites, defined by the crystal structure of the framework, with most observed vacancy diffusion, direct interstitial, and correlated (knock-on) ion transport mechanisms[35]. On the other hand, ionic conductivity of SSEs is proportional to concentration of mobile ions, their charge and mobility. Thus, doping, or elemental substitution can affect both mobility and concentration, but also structural distribution of ions, remaining a powerful tool to optimize electrochemical performance of SSEs. At the nanometer to micrometer scale, microstructural features such as grain boundaries, pores and other higher order defects can affect the ion transport significantly, in many cases detrimentally.

Modern data-driven perspective approaches the problem of ionic diffusivity by using ion descriptors to model and understand which properties affect ionic diffusion[37]. Such an investigation enabled the construction of a database for the analyses of 61 materials with different mobile ions consisting of 46% Li-, 23% halides-, 15% Na-, 8% O- and 8% Ag/Cu-containing structures. A total of 54 computed descriptors were divided into the categories of mechanical-elastic (based on Density Functional Theory, DFT, data), diffusive-vibrational (DFT), and structural-compositional (Ab-initio molecular dynamics, AIMD), with the inclusion of anharmonic effects from AIMD simulations being highlighted as the most crucial novelty in the work. A statistical correlation analysis does not reveal a single feature to determine diffusion and fully account for the ionic behavior, rather a collection of 19 out of 53 features (diffusion coefficient discarded) with an absolute Spearman correlation of over 20%. The correlation study indicates that insulators with small average phonon frequencies, large heat capacity and large vibrational entropy are promising ionic conducting candidates. Several neural networks are trained using only DFT descriptors and a scheme including AIMD descriptors to predict the ionic diffusion coefficient, volume heat capacity C_v and mean vibrational frequency $<\omega>$. The predictions of $<\omega>$ and C_v can be significantly improved when including the AIMD descriptors, yielding low mean-absolute-percentage-error (MAPE) on the test set of 0.061 for C_v, and 0.3 for $<\omega>$ predictions. While the more interesting diffusion coefficient prediction is improved by including all descriptors going from test MAPE: 2.8, train MAPE: 1.4 to test MAPE: 2.6, train MAPE: 0.79, though unfortunately with the MAPE score remaining extremely high. While potassium ionic conductors are not included, the universality of the study and inclusion of anharmonic descriptors remain relevant.

While considerable amount of research has been done on oxide-based transition-metal doped K^+ ionic conductors such as doped and undoped $KFeO_2$, most oxides offer reasonable conductivities in the 10^{-4} to 10^{-2} S cm^{-1} range only at high temperatures around 300–400 °C, making them unsuitable for the use in all solid-state batteries (ASSBs)[38]. Ionic conductivity of potassium ions in oxides has also been the subject of high-throughput screening. 374 ternary and quaternary ionic conducting candidates were reported in ref. 39, where a Voronoi partition method was applied to 1957 crystal structures. The approach computes infinite migration maps for the K^+ cation in the one-, two- and three-periodic case, if they exist in the computed Voronoi partition of the structure. A total of 18 structures are investigated further using the nudged elastic band (NEB) DFT method to compute the migration energies with 4 structures already having been reported to be ionic conductors, although predominantly mixed conductors suitable to be used as electrodes. The four known structures and their minimal path migration energy in each periodic type are proposed based on comparable migration barriers to the known conductors analyzed as can be seen in Table 1.

In another study, high-throughput screening of potassium containing oxides has been performed using bond valence calculations in which K^+ ions are assumed to move within stationary anions and cations[40]. A bond valence computed migration energy of 0.96 eV is set as a screening criterion, only allowing for 22 structures with lower migration energy to proceed. A subsequent ab initio molecular dynamics computation shows both a low migration energy barrier and a large mean square displacement for K_2CdO_2. Subsequent NEB calculations yield a migration energy barrier of 0.40 meV for vacancy-assisted movement, while energy of interstitial-assisted mechanism was reported to be 0.13 meV. However, a formation energy of 0.29 eV for one charged interstitial site limits the realization of the above-mentioned mechanism.

Most of the known ionic conductors with viable room temperature conductivities and lowest E_A can be classified as derivatives of known Li^+ or Na^+ ionic conductors (for example K_3SbS_4 and K-β''−Al_2O_3). Though their E_A is comparable, their ionic conductivity is still significantly lower than some of the best-known Li and Na-based electrolytes ($Li_7Si_2S_7I$, 1.0×10^{-2} S cm^{-1}, $Li_{9.54}Si_{1.74}P_{1.44}S_{11.7}Cl_{0.3}$, 2.5×10^{-2} S cm^{-1},[41] and $Na_{2.88}Sb_{0.88}W_{0.12}S_4$, 3.2×10^{-2} S cm^{-1},[42]). Figure 1 lists the K^+-ion conductivities of known materials and the respective E_A of solid electrolytes with highest ionic conductivity σ_{ion} at RT (for detailed data and references see table S2 (SI)). While materials like $K_{0.4}Cd_{0.3}FeO_2$ and $K_{07}Sr_{0.15}GaO_2$ offer excellent σ_{ion} at elevated temperatures (3.4×10^{-2} S cm^{-1} and 2.1×10^{-2} S cm^{-1} at 400 °C), this review will focus on electrolytes with reasonable (near) RT σ_{ion}. Prospective electrode materials, for example layered oxides[43], have been excluded as they typically show both ionic and electronic conductivity, the latter of which is undesirable for electrolytes which should be purely ionic conductors. The highest room temperature ionic conductivity (3.5×10^2 S cm^{-1}) and lowest E_A (0.08 eV) has been reported for single crystalline $K_2Fe_4O_7$, however this material is expected to be a mixed conductor, as its bandgap is predicted to be 1.32 eV[44]. Albrecht et. al. reported the formation of a $K_{1.7}Fe_4O_{6.7}(OH)_{0.3}$ hydroxide of the same space group and with near identical lattice parameters under similar synthesis conditions[45,46]. A substantial hydrogen content was observed via carrier gas hot extraction as well as a recorded loss of water during heating at 200 °C via thermogravimetry mass spectroscopy (TG-MS), while no mass loss during heating to 800 °C was reported for $K_2Fe_4O_7$. The presence of hydroxide ions and residual crystal water from the hydrothermal synthesis could explain both the reported high ionic conductivity as well as the low E_A of $K_2Fe_4O_7$.

Table 1 | Minimal 1,2 and 3-dimensional path migration energies of known and potential K^+ ion conductors, based on nudged elastic band density functional theory calculations[39]

Structure	Minimal path migration energy [eV]		
	1D	2D	3D
$KFeO_2$	0.106	0.155	0.227
$KAlO_2$	0.094	0.135	0.257
$K_2Cu_3Ge_5O_{14}$	0.261	0.883	
K_2SbPO_6	0.292	0.359	0.668
$K_5As_3O_{10}$	0.279	0.300	0.425
$K_4V_2O_7$	0.218	0.341	0.388
$K_2Zn_3O_4$	0.064	-	-
$K_2Sb_4O_{11}$	0.096	-	-
$K_3NbAs_2O_9$	0.130	-	0.611
$K_3NbP_2O_9$	0.195	-	0.774
$K_2Al_2Sb_2O_7$	-	0.141	-
$K_6CuSi_2O_8$	0.240	0.463	0.512

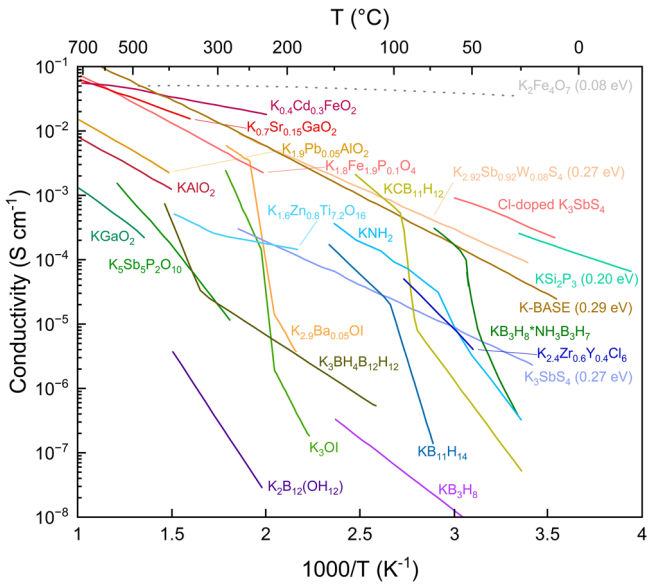

Fig. 1 | Temperature-dependent conductivity of various K^+ solid electrolytes together with E_A of selected compounds. The data for $K_2Fe_4O_7$ is obtained from single-crystal measurements. K-BASE denotes a sample consisting of 91 wt% K-β"-Al_2O_3, 8.4 wt% K-β-Al_2O_3, and 0.6 wt% ZrO_2. $K_2Fe_4O_7$ is included as the electrolyte with the currently best reported RT σ_{ion} and E_A, but those might be partially from H^+ conduction as well as crystal water. The ionic conductivities are summarized from[42,49,58,60,65,90–104]. Detailed references can be found in Table S2 (SI).

This structure has not been reported experimentally for the Li and Na case, possibly as due to a tendency to decompose into Li- or $NaFeO_2$ and Fe_2O_3[47,48].For some of the ionic conductors like K-BASE, which consists of K-β"$-Al_2O_3$ with minor amounts of K-β-Al_2O_3 and ZrO_2, existence of such additional poorly conductive phases is necessary in the material entering battery cell as the mechanical integrity of pure K-β"$-Al_2O_3$ is too low for practical applications[49].

K^+ electrolytes derived from Li^+ or Na^+ conductors usually need a volumetric adaptation of the lattice to accommodate the larger K^+ cation. Examples are K_3SbS_4, derived from Na_3PS_4, as well as K_3OI, derived from Li_3OCl. This is done via partial substitution with bigger ions, for example Sb^{5+} instead of P^{5+}, I^- instead of Cl^-, or K^+ instead of Na^+ in K-β"-alumina. In some case, structures such as K_3OCl[50] and K_6PS_5Cl[51], which are similar to the known solid electrolytes Li_3OCl[52], Na_3OCl[53], Li_6PS_5Cl[54] and Na_6PS_5Cl[55] are shown to be synthetically obtainable, but their ionic conductivities have not yet been tested. In the K_3OI anti-perovskite, which is structurally identical to conventional perovskites but with inverted cation and anion sites, ab initio methods were employed to understand the diffusion and an experimentally observed phase-change. Modelling conductivity for the K_3OI structure reveals that the existence of vacancies is crucial for the ion-diffusion observed. By computing probability distribution function of the ionic species, the study shows a high-temperature disorder in the I-O sublattice with a low activation energy (0.76 eV through NEB) compared to that of the K-ion. This is believed to be the observed phase-change, which causes the ions to diffuse through the local gaps of I-O disorder and vacancies.

Generally, body-centered cubic (bcc) anion sublattices seem to be beneficial for fast ion conduction as cations can hop between energetically equivalent adjacent tetrahedral sites, while in face-centered cubic (fcc) and hexagonal close-packed (hcp) sublattices ion migration occurs through higher energy octahedral sites[56]. This rationale has been demonstrated to be favorable for fast Li^+ and Na^+ migration in, for example, $Li_{10}GeP_2S_{12}$ and $Li_7P_3S_{11}$ and can also be applied for potassium. Na_3PS_4 and W-doped Na_3SbS_4 display similarly high $\sigma_{ion} > 10^{-4}$ S cm^{-1} at RT compared to W-doped $K_{2.92}Sb_{0.92}W_{0.08}S_4$ $\sigma_{ion} = 7.7 \times 10^{-5}$ S cm^{-1},[42,57]. Newly reported Cl-doped K_3SbS_4 shows a record RT conductivity $\sigma_{ion} = 3.2 \times 10^{-4}$ S cm^{-1} linked with low $E_A = 0.26$ eV[58]. This class of materials consists of a bcc anion framework of the PS_4^{3-} or SbS_4^{3-} tetrahedra, which is slightly distorted for K_3SbS_4.

Depending on the crystal structure, K^+ migration can predominantly occur through 2D or 3D pathways. The K- β"-Al_2O_3 structure consists of alternatively stacked non-conducting Al_2O_3 spinel blocks, separated by loosely packed layers of potassium oxide which form conduction planes and allow for K^+ transport. It has been experimentally observed that the room-temperature σ_{ion} of K-beta"-Al_2O_3 is higher compared to Li and Na counterparts. Recently, a DFT study showed that in these materials, vacancy mechanisms dominate, meaning that the occupation of the conduction plane sites determines the σ_{ion}[59]. In the orthorhombic K_3SbS_4, K^+ migration is through void sides, resulting in a two-dimensional diffusion network, while the open 3D framework of $K_2Fe_4O_7$ consists of 2D 6-ring channels parallel to the *a* and *b* axis, filled with highly disordered K^+ cations (Fig. 2b, c). The σ_{ion} of single crystals along the *a* axis was reported to be up to 5×10^2 S cm^{-1} at 500 °C (5 S cm^{-1} along the *c* axis at the same temperature), demonstrating the highly anisotropic σ_{ion}, a consequence of sufficiently open channels of optimal size along the *a* axis and smaller openings between two FeO_6 octahedra and one FeO_4 tetrahedra along the *c* axis.

Another interesting electrolyte is T5 KSi_2P_3 as it also has a good room temperature $\sigma_{ion} = 2.6 \times 10^{-4}$ S cm^{-1} and an interesting structure consisting of a network of interconnected five SiP_4 tetrahedra long supertetrahedra (Fig. 2d)[60]. The voids of this network are filled by a second crystallographically identical network, with the K^+ residing in the big cavities between the two networks. The eleven K^+ positions have an average occupancy of 0.4 and are thus disordered, leading to a high mobility of the K^+ ions at room temperature through isotropic 3D channels along the supertetrahedra.

It should be noted that for oxide and sulfide-based solid-state ionic conductors, doping has been shown as beneficial for transport performance as it creates additional vacancies which boost σ_{ion}. This can either be done by modifying the anion lattice, for example by partially replacing Sb^{5+} with W^{6+} for K_3SbS_4 or by introducing aliovalent cations of a similar size to K^+. For example, Ba^{2+}−doped $K_{2.9}Ba_{0.05}OI$ has a reported $\sigma_{ion} = 3.5 \times 10^{-3}$ S cm^{-1} at 270 °C and crystallizes in the antiperovskite structure. The Li compound $Li_{3-2x}Ba_xOCl$ (x = 0.005) is also an excellent ionic conductor ($\sigma_{ion} = 2.5 \times 10^{-2}$ S cm^{-1} at RT). Similarly, to mitigate the energy necessary for carrier creation an Al-doping is proposed at Cd sites in K_2CdO_2 for which they report a migration energy barrier of 0.42 ± 0.03 eV with $\sigma_{ion} = 2.2 \times 10^{-5}$ S cm^{-1} at 27 °C[40]. A computational study was conducted on the doping effect of Ti in structurally similar $KFeO_2$[61]. Here all inequivalent atomic arrangements with minimal Ti doping ($x = 0.03$, $x = 0.06$, $x = 0.09$)

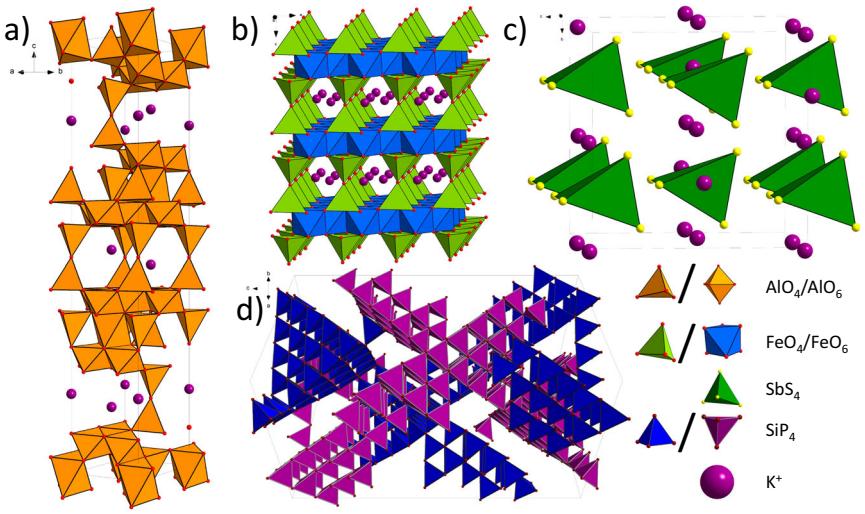

Fig. 2 | Crystal structures of promising solid-state potassium electrolytes. a K-β''-Al_2O_3, **b** $K_2Fe_4O_7$, **c** K_3SbS_4, **d** KSi_2P_3 with K^+ diffusion along the ab-plane for K-β''-Al_2O_3, along channels for $K_2Fe_4O_7$ (along the b-axis) and K_3SbS_4 (along the c-axis) and the 3D ionic conductor KSi_2P_3. This figure was drawn using the program Diamond Version 5.0.0.

in $K_{1-x}Fe_{1-x}Ti_xO_2$ are generated along with all migration pathways for the three dopant cases. For the $x = 0.03$ case, all K^+ migration energy barriers were computed using the NEB method, properties such as pathway dopant distance and angles were used as descriptors for a machine learning model using ridge regression and ensemble-based (gradient boosting and random forest) regression aiming to predict the maximum energy of the pathways. In the study, the pathway dopant angle is concluded to have a large effect on the K^+ ion diffusion perhaps due to the doping effect on the crystal structures' lability. The pathway dopant distance did not have a large impact on the migration, therefore no indication of a decisive electrostatic role of the dopant on the K^+ migration.

Metal borates have been getting an increased amount of attention as a possible SSE candidate, however only at elevated temperatures. The special cases of closo-dodecaborates $M_2B_{12}H_{12}$ (M = Li, Na, K), are also analyzed by ab initio methods[62]. The aim is to model the electronic, ionic, vibrational, and thermodynamic properties of the materials, of which ionic conductivity for the $LiB_{12}H_{12}$, $NaB_{12}H_{12}$, and even $LiNaB_{12}H_{12}$ cases have been reported. Furthermore, the high-temperature superionic phase of $Na_2B_{12}H_{12}$ has been shown to exhibit rapid reorientation dynamics of the $B_{12}H_{12}^{2-}$ anion aiding the cation motion. However, the reported computed E_A in the potassium case is 1.25 eV, compared to 0.7 eV and 1.16 eV for Li and Na respectively. A large insulator bandgap of 5.59 eV is reported in the case of $K_2B_{12}H_{12}$. Additionally, MD simulations demonstrated the material to be stable at 300 K and 600 K, with thermal stability being a general necessary property needed for potential SSEs.

Anode/electrolyte interfaces in K-based solid-state batteries

One of the main issues to be addressed in high energy K-based solid-state batteries is the adhesion of K metal and the solid-state electrolyte as well as related interfacial reactivity. Electrochemical impedance spectroscopy (EIS) is possibly the most relevant in situ diagnostic tool to track the (electro)chemical degradation pathways and state-of-health (SOH) via voids formation, interfacial contact area decreases, creep through the impedance increase or decrease, respectively, combined with an informed mechanistic model[63].

To achieve high critical currents, the interfacial resistance needs to be minimized to reduce its detrimental effect on K^+ ion transport. For K-β''-Al_2O_3, it could be demonstrated that polishing and heat-treatment could reduce the interfacial resistance between K-β''-Al_2O_3 and the potassium electrodes. Figure 3a shows the Nyquist plot of a K/K-β''-Al_2O_3/K cell after heat-treatment at different temperatures under Ar. Depending on the heat-treatment temperature, the interfacial resistance could be decreased by an order of magnitude (Fig. 3c) which could be attributed to a loss of surficial hydroxide and carbonates.

Critical currents for dendrite penetration and voiding in potassium metal anode SSBs are usually higher than those in similar Li- and Na-systems due to lower yield strengths and therefore more pronounced creep of potassium[64]. For K-β''-Al_2O_3, the critical current for dendrite formation of 4.8 mA cm^{-2} is among the highest reported for a metal anode/SSE interface. However, it should be noted that the critical current density for voiding in this system is reported to be as low as 2 mA cm^{-2}, as can be seen in Fig. 3d, e. This leads to a decreased contact area between the metal anode and solid electrolyte (SE), localized higher current densities, and dendrite formation at those positions.

Interfacial stability between the SE and electrodes is another challenge, especially for K metal electrodes. Zheng et al. demonstrated that Ba^{2+} doped antiperovskite K_3OI shows excellent stability against K metal as its anions cannot be further reduced by K metal or K^+ containing anodes, but its high phase transition temperature of 240 °C is needed for good σ_{ion}[65]. In addition, the observed high charge transfer resistance is expected to limit its applications in real systems. The interfacial stability of borohydride complexes such as $KB_3H_8{\cdot}NH_3B_3H_7$, which incorporate a neutral $NH_3B_3H_7$ molecule to achieve higher σ_{ion} of 1.3×10^{-4} S cm^{-1} and cationic transference number, $t_{K+} = 0.93$ has also been investigated. This material exhibits good initial interfacial stability against K metal, however, the formation of unknown decomposition products was visible after 166 cycles.

The interfacial stability of oxide based Na-BASE against Na metal was confirmed via X-ray photoelectron spectroscopy (XPS)[66]. Comparable stability of K-BASE against K is expected as a K-S cell with a K-BASE electrolyte showed excellent cycle stability over 1000 cycles[49]. For solid electrolytes with sulfides, such as K_3SbS_4, formation of a potassium-sulfide based SEI is expected, since continuous formation of a Na_2S and Na_3P based interphase has been reported for Na_3PS_4[66]. While sulfides are electronic isolators, the higher electronic conductivity of phosphides can lead to a reduction of the electrolyte and constant growth of the SEI[67]. As the volume fraction of phosphides in K_3PS_4 is supposed to be lower than sulfides, an encasement of isolated K_3P clusters in a sulfide-based matrix is possible. The formation of electronically conducting interphases may be a problem for K_3SbS_4 and especially KSi_2P_3 as potassium-antimony compounds may show a higher electronic conductivity than their phosphide analogues. In addition, the formation of potassium-silicon compounds has only been reported at elevated temperatures and pressures.

Contemporary characterization techniques

X-ray powder diffraction

X-ray powder diffraction is widely used for compound identification when new materials are synthesized. In addition, Rietveld refinement (such as in Fig. 4a) can be used for quantitative analysis of crystalline phases and

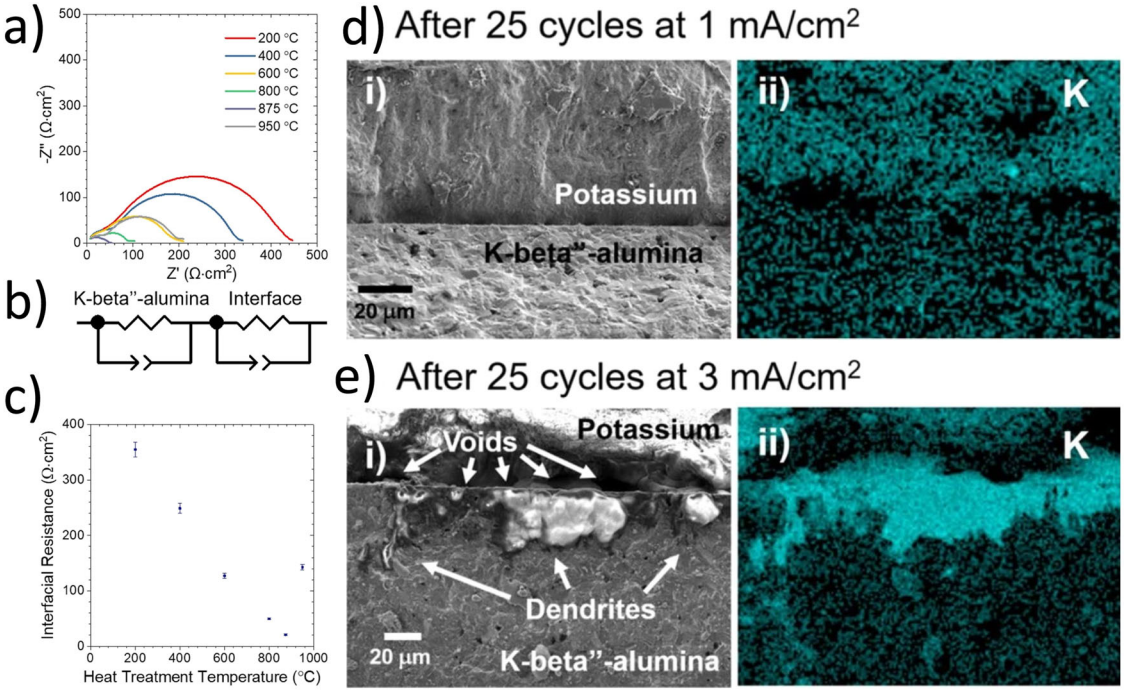

Fig. 3 | Interfacial properties of K-β''-Al_2O_3 as measured from symmetric K cells cycled at 20 °C. a Nyquist plot of symmetric K/K-β''-Al_2O_3/K cell after heat-treatment at different temperatures under Ar, **b** equivalent circuit model used for the determination of the interfacial resistance, **c** plot showing the modelled interfacial resistance against heat treatment temperature and **d**, **e** showing scanning electron microscopy (SEM) images and energy dispersive X-ray spectroscopy (EDX) mapping of K (turquoise) of the K/K-β''-Al_2O_3 interface after 25 cycles. Reproduced with permission from[105].

amorphous content as well as refinement of crystal structures. Due to its non-destructive nature, low sample demand (in the mg range) and ability to do fast in situ measurements in special cells, it has become a standard method in the lab. While it is an excellent method for structure refinement and in situ studies (for example the change in lattice parameters due to Li/K intercalation or doping) due to its high 2θ resolution and therefore accurate determination of lattice parameters, an unambiguous structure solution is often difficult or factually impossible as symmetry-equivalent reflections have the same d spacing. As the scattering intensity depends on the atomic number Z, K^+ occupancy should be easier to determine compared to Li^+ due to the higher scattering intensity. While a plethora of information like the weight fraction of crystalline compounds (and amorphous phases), their lattice parameters, occupancy, crystallite size and strain can be extracted, accurate Rietveld refinements, especially in multi-component systems still require a fair bit of experience and can hardly be automatized. Data representation of Rietveld refinements should clearly state which parameters were refined (e.g., atomic positions, structural, microstructural, and thermal displacement parameters) and according to which order. The observed pattern, fit profile, difference curve and reflection positions should be clearly visible. In addition, chemical compositions calculated from occupancy should be cross-checked using other characterization methods, such as inductively coupled plasma mass spectrometry (ICP-MS) of solutions. For structure solution, single crystal X-ray diffraction (SXRD) is usually required as it measures the intensity as a function of the Miller indices hkl compared to d spacing for powder XRD and enables an unambiguous space group determination. Neutron powder diffraction can serve as a complementary method as its scattering intensities rely on the scattering length and not on the Z of ions.

Neutron techniques

Multiple neutron absorption and scattering methods are increasing in popularity in the investigation of solid-state battery materials. Neutron powder diffraction (NPD), neutron tomography, quasielastic neutron scattering (QENS) and inelastic neutron scattering (INS) are among the most commonly used, offering in-operando and in-situ experiments with outstandingly flexible sample environments (see ref. 68 for a review). The application of these methods allows for the determination of atomic structure, atomic positions, and diffusion pathways using diffraction techniques similar to those performed with X-rays[69–71]. INS and QENS methods allow the determination of re-orientational dynamics and the understanding of the physical mechanisms of diffusion dynamics[72].To the day, most reported investigations using neutron methods in K-solid-state battery materials are focused on electrodes. This could be due to multiple electrolyte compounds (such as the ones listed in Fig. 1) containing boron, gadolinium, cadmium, and antimony, which show large neutron absorption cross sections, making the experiments more difficult. Besides, the hydrogen content with a remarkably high incoherent cross-section, can hinder the observation of coherent potassium signal. Dimitrievska et. al. report on QENS and INS results on $KCB_{11}H_{12}$[73] specifying the use of an ultra-thin sample geometry to avoid these issues. From the neutron data, it could be concluded that the anion diffusive jump frequencies are very small in comparison to over-damped vibrational frequencies with a motion of 0.41(3) Å. The comparison of these results for K with those for Li and Na, show a consistent correlation between cation size and anion reorientation jump rates. Another example on the use of QENS and INS is presented by Andersson et. al. for KB_3H_8[72], where a clear connection can be made between the local structure (determined by X-rays) and the reorientation dynamics. In this study, use of ultrathin samples for QENS experiments and reflection geometry for the INS experiments has also been mentioned.

Electrochemical impedance spectroscopy

Electrochemical impedance spectroscopy (EIS) is an invaluable in situ tool for studying electrochemical systems as it can deconvolute electrochemical processes in the cells by their different relaxation time. In batteries, those processes (e.g., electron transfer from the current collector to the electrode, electron conduction across the electrode, ion migration across the electrode, insertion of ions and electrons into active particles, double layer charging at solid/liquid interfaces, coupled ion diffusion in the active particle and

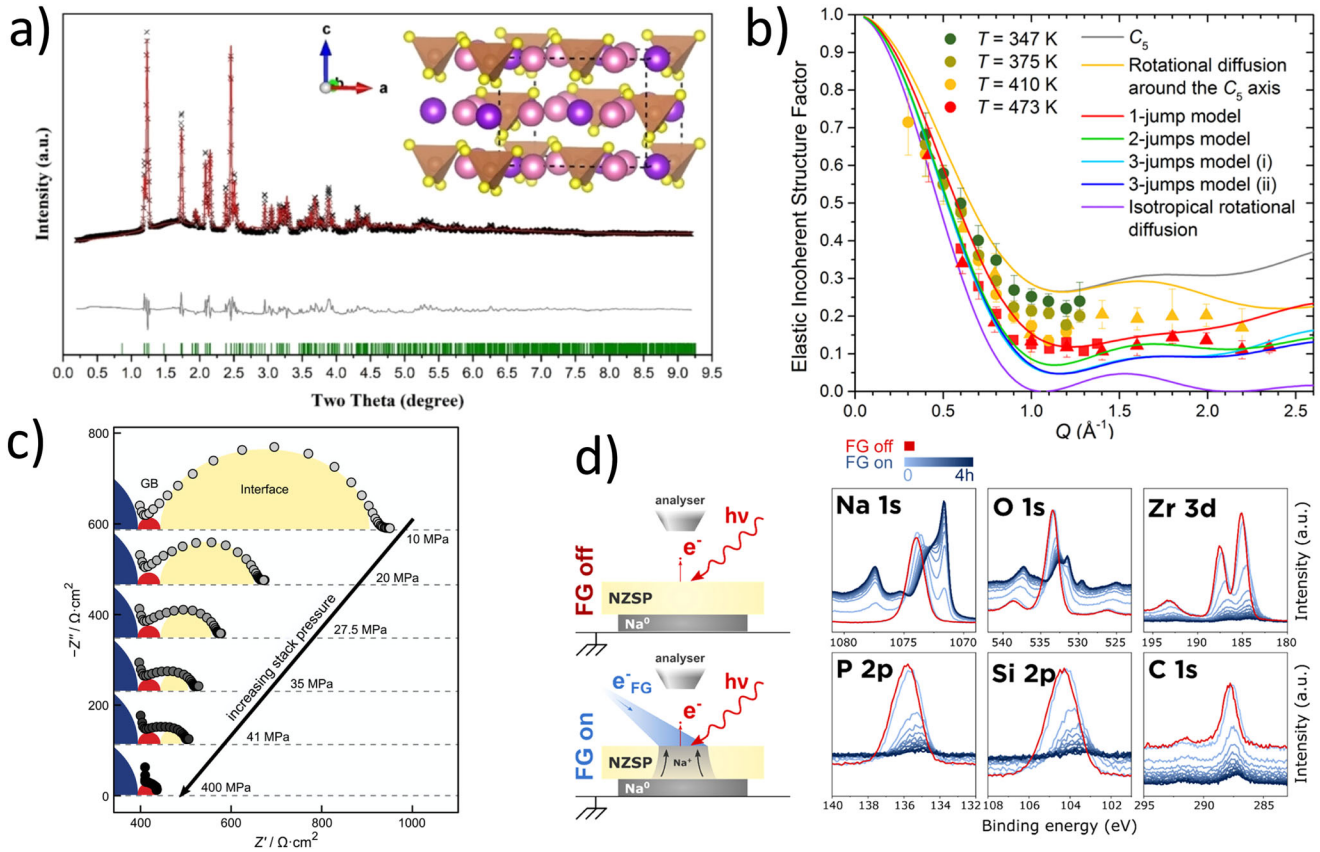

Fig. 4 | Contemporary characterization techniques. a Rietveld refinement of SXRD data and crystal structure for orthorhombic *b*-K_3SbS_4. Reproduced with permission from **b** elastic incoherent structure factor vs the neutron momentum transfer **Q** of $KCB_{11}H_{12}$ at different temperatures, derived from quasielastic neutron scattering (QENS) measurements with model curves for various anion reoriental mechanisms for comparison. Reproduced with permission from[73]. **c** EIS data on the pressure dependence of the interface impedance of a symmetric Li|$Li_7La_3Zr_2O_{12}$(LLZO)|Li cell. Reproduced with permission from[77] **d** Demonstration of the working principle of the *operando* plating of Na on the solid electrolyte $Na_{3.4}Zr_2Si_{2.4}P_{0.6}O_{12}$ by using the flood gun as an electron source inside a XPS to study the interphase formation between the SE and a Na electrode. Reproduced with permission from ref. 106.

electrode and migration/diffusion of ions in the separator and others) often overlap, making an unambiguous assignment of features of the impedance spectrum challenging[74,75]. Methods for reducing the number of observed processes, like the use of symmetric cells with two identical electrodes (where the interfacial processes are expected to be symmetric), change of temperature, and the use of ion-blocking electrodes especially for the separation of the bulk and grain boundary are some of the possible solutions[76]. Eckhardt et al. demonstrated that geometric current constriction due to poor contact between electrode and solid electrolyte resistance can even dominate the interfacial properties, especially in the case of an interface with a rigid electrolyte such as Li-LLZO system and proposed a strategy for the identification of interfacial processes via EIS in chemically stable systems (no considerable SEI evolution). By measuring impedance at different stack pressures and performance of a distribution of relaxation times (DRT) analysis, the influence of the bulk, grain-boundary resistance, geometric current constriction and charge-transfer resistance can be separated, and the rate-limiting process identified(see Fig. 4c)[77]. In full cells, separating the contributions from anode and cathode can be difficult and while the use of reference electrodes (RE) has been common for liquid cells, they have not been widespread in solid-state batteries. Sedlmeier et. al. and Hertle et. al. showed that 64 µm thick gold-wires and 10 µm thick gold-plated tungsten wires can be embedded in Li_6PS_5Cl and used as reference electrodes in solid state batteries[78,79]. By applying a small current (and with negligible charges in the µAh range) against a Li or In/Li anode, a gold wire can be in situ lithiated to form a reference electrode (RE). By measuring the impedance of the individual electrodes against RE as well as by comparison of the full cell impedance with the sum of the two measurements against RE the contributions of the individual electrodes can be determined. The same method should also be applicable for other alkali metals and enables the convenient use of a RE with minimal changes to the cell geometry.

Nuclear magnetic resonance

Solid-state nuclear magnetic resonance (ssNMR) can probe both local structure and ionic motion, which was implemented in many battery materials, including oxide-type solid state electrolytes[80]. However, in the case of ^{39}K ssNMR, the quadrupolar coupling constants are high, leading to central transitions, thus studying materials at high magnetic fields (above 21 T) is necessary[81]. Another way to reduce the central transition line width is by magic angle spinning[82]. The sensitivity can be increased by quadrupolar echo NMR during a Carr-Purcell-Meiboom-Gill train, as shown on $K[BPh_4]$[83]. The complexity of such experiments results in the fact that chemical shift anisotropy (CSA) parameters have been reported rarely, for any K-containing samples[83,84]. Relative chemical shifts are known for some borate glasses[85]. Most recently, when investigating K_2SnCl_6 compound, DFT analysis helped predict the CSA parameters[86]. Simulation of ^{39}K ssNMR spectra of pristine and Cl-doped K_3SbS_4 shows subtle changes in ratios of mobile K1 and immobile K2 sites[58].

In situ/*operando* techniques

As most processes in batteries which limit their performance happen at the electrode/electrolyte interface like the formation of SEIs, voids, dendrites, in situ and *operando* measurements are crucial for understanding interfacial evolution and reaction mechanisms in working batteries. One of the promising ones would, for example, be in situ[87] or operando XPS (Fig. 4d) where

chemical aspects can be determined precisely. Ex situ/post-mortem techniques like XPS or time-of-flight secondary ion mass spectrometry (TOF-SIMS) and atom probe tomography require disassembly of the cell and exposition of the buried interface to an atmosphere, which is experimentally difficult in the solid-state and may change the composition (to the kinetically stabilized phases) or morphology of it in the process.

Few studies of potassium solid-state batteries employ XPS such as the one by Shao et al. where SO_2 and polysulfide species were characterized at the cathode of a K | $K_{2.92}Sb_{0.92}W_{0.08}S_4$ | S battery. It has furthermore been demonstrated that due to a higher ionization potential of potassium and a more pronounced screening effect than for Li and Na the observed binding energy may change significantly. For instance, the binding energy value of the C 1 s peak of K_2CO_3 is typical of the C 1 s peak of RCO_2Li, potentially leading to misidentification[88]. Most in situ techniques like optical, electron or scanning probe microscopy require specially designed electrochemical cells where care must be taken that the conditions in those cells resemble real battery cells.

Conclusions and outlook

Development of inorganic SSEs remains one of the most important materials challenges for enabling commercialization of solid-state batteries. In K-based chemistries, several classes of electrolytes (sulfide, oxide, and phosphidosilicates) show promising bulk (low activation energy and relatively high RT ionic conductivity) and interfacial electrochemical performance (stable cycling for up to 1000 of cycles).

For the new synthesis routes of new K-electrolytes with high σ_{ion}, inspiration can be drawn from their Li/Na analogues where change of the synthesis conditions and thus $c_{defects}$ significantly improved room temperature σ_{ion}. In addition, traditional high temperature synthesis leads to relatively low σ_{ion}, while a harsh mechanochemical synthesis via ball-milling is known to introduce defects, leading to around an order of magnitude higher σ_{ion}. It should, therefore, be noted that for the search for new potassium ionic conductors, the structure of electrolyte, doping/vacancy concentration as well as the synthesis methods play an important role, in particular when other phases or water might be present in the structure. Reproducibility of synthesis routes as well as detailed description of materials' handling outside of inert gas environments prior to electrochemical measurements remains non-addressed in many cases. Similarly, as effect of internal strain and dislocations due to applied pressure have also been shown to be beneficial to Li^+ conduction, these should also merit consideration for the potassium case.

The effects of nanoconfinement on the ionic conductivity of potassium borohydrides might be worth exploring, as pure KBH_4 is unsuitable as a SSE due to its low RT ionic conductivity in the 10^{-11} S cm^{-1} range. In the lithium case, the nanoconfinement of $LiBH_4$ into various oxides yielded a σ_{ion} increase of four orders of magnitude due to the introduction of space charge effects. Those effects are expected to be even more pronounced for the potassium case due to its lower ionic conductivity, making it a potentially viable electrolyte.

Anti-perovskites have been the subject of many computational studies for SSEs for various charge carriers. However, there seems to be a gap in the literature, when it specifically comes to computational studies focusing on potassium. An example of a more recent accelerated workflow investigating Li, Na and Mg containing anti-perovskites combined ab initio methods with machine learning (ML) to obtain thermodynamic and electrochemical stability, ionic diffusivity, and semiconductance. To accelerate the computationally heavy NEB calculations, a surrogate model was employed to predict transition states during diffusion. The Li, Na, and Mg candidates identified in the study as potential SSE have all already been discovered to be ionic conductors, which highlights why an inclusion of K in the future would be interesting.

Recent advances in superionic conductivity have shown that a corner-sharing framework can promote ionic conduction effectively. Computational screenings investigating this trend have not been pursued for potassium-containing oxides yet, although Materials Project does report negative formation energies for $K_{1+x}Al_xTi_{2-x}(PO_4)_3$ and KTa_2PO_8, but it would no doubt be beneficial for the community since the continuous symmetry measure (CSM) of crystal structures, which quantifies how distorted polyhedrons are from their perfect counterpart (CSM = 0), have been shown to be an important parameter determining the structural capability for superionic conductance.

In terms of interfacial characterization, this field is in its infancy, and much is yet to be understood on how the specificities of structure, pressure dependence of electrochemical properties of K-SSEs, and their behavior in contact with K metal may be further tuned to allow for high-energy density cells with long enough lifetime. Here, new and revived spectroscopic and diffraction techniques, preferably applied in situ and *operando*, play a crucial role in elucidating ion transport mechanisms at different time scales, as well as chemical changes at different length scales, from atomic to battery cell level. For example, three-electrode cells can be used to separately study the processes of stripping and plating of alkali metals. Optical microscopy can potentially be used to study deposition/dissolution and the growth of dendrites on the μm scale but requires a cell design where one side of the cell is open to the visible light. In situ electron microscopy techniques have been used to study the morphology, plating and evolution of lithium dendrites in solid electrolytes during cycling, but *operando* measurements of potassium remain challenging due to the required thin films for transmission setups and the low electron beam damage threshold of potassium, necessitating the use of cryo-stages. Electrochemical atomic force microscopy may be used to study the morphology of the cathode electrolyte interface in potassium solid state batteries on the nm scale, but its temporal resolution due to the time required for a single scan limits its use as an *operando* method.

Computational studies dedicated to electrolyte/electrode all-solid-state interfaces for potassium ion batteries are currently close to non-existent. Due to the complexity of interphases compared to the bulk properties, computational studies will usually limit the work to a single ionic type. Ab-initio assessment on the electrochemical stability window and thermodynamic phase equilibria of proposed K^+ ionic conductors, similarly to the work on Na^+ conductors, is necessary to further the potential of potassium SSB. The existence, and relevance of space charge layers for SSBs has been discussed as it can potentially affect the SSE interfaces with cathode and anode. If relevant, the effects are to be similarly present in the Na and K-case with the easiest indicator being increase/decrease of measured activation energy of ion transport compared to the bulk.

Modeling studies of superionic conductance tend to assume a static framework of anions in which the cations move, recent findings however suggest that there is much to learn about the influence of the effect anion rotational dynamics has on the diffusivity of the cations. Structures that exhibit the rotor phase, however, rarely do so at the low temperatures necessary for SSE, and even predicting which materials might have this property is currently not possible. Rotor phases in inorganic salts such as anti-perovskite $[BH_4]^-$, closo-borates and carba-closo-borates ($[B_{10}H_{10}]^{2-}$, $[CB_9H_{10}]^-$, $[B_{12}H_{12}]^{2-}$, $[CB_{11}H_{12}]^-$), phosphates ($[PO_4]^{3-}$), sulfates ($[SO_4]^{2-}$) and thiophosphates ($[SiS_4]^{4-}$, $[PS_4]^{3-}$, $[PSe_4]^{3-}$) have been shown to contribute to Li^+ and Na^+ diffusion via the paddle-wheel effect as well as in $K_{3-2x}M_xPO_4$ (M = Mg, Ca, Sr, Ba Zn, Cd, Pb) and $K_{3-x}P_{1-x}E_xO_4$ (E = S, Cr, Mo, W) in data analysis due to orientation disorder of the PO_4 tetrahedra. Further exploration into the paddle-wheel effect can potentially lead to insights in potassium ionic conductors and might already be a contributing factor in several known conductors.

The conductivity of crystalline material at the mesoscale can be modeled through kinetic Monte Carlo (kMC). In this method, a stochastic ensemble of ionic migration enables the evaluation of the transition rate of different events, which allows for extraction of the conductivity through the Einstein relation in a kMC simulation. This method is however yet to be applied to SSEs for potassium batteries.

The modeling and computational research conducted for electrode-electrolyte interfaces for solid-state potassium batteries is limited. The challenges for potassium are expected to be similar, but the subject is not as mature as lithium-based systems. Currently, most necessary is to screen

electrolyte materials with a large electrochemical window allowing for utilization of high-voltage cathode materials. The electrochemical stability window can be investigated by subjecting the electrolytes to the chemical potential of the charge carrier, to gain general insight into battery performance. For more complex interfaces, reaction energies for possible intermediate phases might also be worth exploring. While the methodology itself can be completed entirely from experimental thermodynamic data, DFT results can be added. The methodology was applied to known solid-state electrolytes for lithium batteries and suggested promising cathode-electrolyte combinations that had not yet been reported experimentally. DFT can be used to investigate defects related to the interface of alkali metal and solid electrolyte. In the case of lithium, the model leads to a formation of a thin disordered layer at the interface, which can cause pore formation. The study finds lattice mismatches of the metallic anode and SE to play a crucial role in the general cyclability of the interface. Applying the same methodology for potassium-based systems could be beneficial to gain insight into the difference of shapes and sizes of the expected pores. Similarly as in the case of advanced characterization techniques, there is an urgent need for conceptualization of new computational approaches to aid the solid-state battery development. Unfortunately, few mesoscale and macroscale simulations are performed for solid-state batteries in general.

The implementation of Materials Acceleration Platforms (MAPs) is required for integrated modelling and experimental workflows. On the electrode or electrolyte sides, we are slowly approaching the level of interoperability and automation required by this task. On the interface level, calculations are performed still in a manual fashion and modular workflows are still scarce[89]. Thus, it is necessary to enable a bridging between the various scales (atomic to mm) of a battery. Artificial Intelligence will play a key role here by, e.g., establishing machine learning classical potentials able to extend the time- and length-scales of DFT without losing accuracy or by predicting materials properties.

We have given an overview of the current state of solid-state inorganic electrolytes for potassium batteries, key parameters for good bulk and interface performance as well as contemporary methods of characterizing their performance. We hope that this review will pave the way for discovery, synthesis and characterization of new high-performance SSEs.

Data availability

The authors declare that the data supporting the findings of this study are available within the paper and its Supplementary Information files.

Received: 5 March 2024; Accepted: 10 July 2024;
Published online: 20 July 2024

References

1. Randau, S. et al. Benchmarking the performance of all-solid-state lithium batteries. *Nat. Energy* **5**, 259–270 (2020).
2. Tan, D. H. S., Banerjee, A., Chen, Z. & Meng, Y. S. From nanoscale interface characterization to sustainable energy storage using all-solid-state batteries. *Nat. Nanotechnol.* **15**, 170–180 (2020).
3. Balaish, M. et al. Processing thin but robust electrolytes for solid-state batteries. *Nat. Energy* **6**, 227–239 (2021).
4. Ye, L. & Li, X. A dynamic stability design strategy for lithium metal solid state batteries. *Nature* **593**, 218–222 (2021).
5. Tan, D. H. S. et al. Carbon-free high-loading silicon anodes enabled by sulfide solid electrolytes. *Science* **373**, 1494–1499 (2021).
6. Xiao, Y. et al. Understanding interface stability in solid-state batteries. *Nat. Rev. Mater.* **5**, 105–126 (2020).
7. Zahiri, B. et al. Revealing the role of the cathode–electrolyte interface on solid-state batteries. *Nat. Mater.* **20**, 1392–1400 (2021).
8. Janek, J. & Zeier, W. G. Challenges in speeding up solid-state battery development. *Nat. Energy* **8**, 230–240 (2023).
9. Popovic, J. The importance of electrode interfaces and interphases for rechargeable metal batteries. *Nat. Commun.* **12**, 6240 (2021).
10. Heubner, C. et al. From lithium-metal toward anode-free solid-state batteries: current developments, issues, and challenges. *Adv. Funct. Mater.* **31**, 2106608 (2021).
11. Hatzell, K. B. Anode-less or anode-free? *ACS Energy Lett.* **8**, 4775–4776 (2023).
12. Neudecker, B. J., Dudney, N. J. & Bates, J. B. Lithium-free" thin-film battery with in situ plated Li anode. *J. Electrochem. Soc.* **147**, 517 (2000).
13. Huo, H. & Janek, J. Silicon as emerging anode in solid-state batteries. *ACS Energy Lett.* **7**, 4005–4016 (2022).
14. Sangster, J. K−Si (Potassium-Silicon) system. *J. Phase Equilibria Diffus.* **27**, 190–191 (2006).
15. Lee, S., Jung, S. C. & Han, Y.-K. First-principles molecular dynamics study on ultrafast potassium ion transport in silicon anode. *J. Power Sources* **415**, 119–125 (2019).
16. Kim, K. J., Balaish, M., Wadaguchi, M., Kong, L. & Rupp, J. L. M. Solid-state Li–metal batteries: challenges and horizons of oxide and sulfide solid electrolytes and their interfaces. *Adv. Energy Mater.* **11**, 2002689 (2021).
17. Janek, J. & Zeier, W. G. A solid future for battery development. *Nat. Energy* **1**, 16141 (2016).
18. Ma, J. et al. Interelectrode talk in solid-state lithium-metal batteries. *Adv. Mater.* **35**, 2301892 (2023).
19. Cheng, L. et al. Accelerating electrolyte discovery for energy storage with high-throughput screening. *J. Phys. Chem. Lett.* **6**, 283–291 (2015).
20. Kirklin, S., Meredig, B. & Wolverton, C. High-throughput computational screening of new Li-ion battery anode materials. *Adv. Energy Mater.* **3**, 252–262 (2013).
21. Hautier, G. et al. Phosphates as lithium-ion battery cathodes: an evaluation based on high-throughput ab initio calculations. *Chem. Mater.* **23**, 3495–3508 (2011).
22. Bölle, F. T. et al. Autonomous discovery of materials for intercalation electrodes. *Batteries Supercaps* **3**, 488–498 (2020).
23. Sjølin, B. H. et al. Accelerated workflow for antiperovskite-based solid state electrolytes. *Batteries Supercaps* **6**, e202300041 (2023).
24. Bölle, F. T., Bhowmik, A., Vegge, T., Maria García Lastra, J. & Castelli, I. E. Automatic migration path exploration for multivalent battery cathodes using geometrical descriptors. *Batteries Supercaps* **4**, 1516–1524 (2021).
25. Betz, J. et al. Theoretical versus practical energy: a plea for more transparency in the energy calculation of different rechargeable battery systems. *Adv. Energy Mater.* **9**, 1803170 (2019).
26. Yokoi, R. et al. Potentials and hotspots of post-lithium-ion batteries: environmental impacts and supply risks for sodium- and potassium-ion batteries. *Resour. Conserv. Recycling* **204**, 107526 (2024).
27. Mauler, L., Duffner, F., Zeier, W. G. & Leker, J. Battery cost forecasting: a review of methods and results with an outlook to 2050. *Energy Environ. Sci.* **14**, 4712–4739 (2021).
28. Zaman, W. & Hatzell, K. B. Processing and manufacturing of next generation lithium-based all solid-state batteries. *Curr. Opin. Solid State Mater. Sci.* **26**, 101003 (2022).
29. Batzer, M., Heck, C., Michalowski, P. & Kwade, A. Current status of formulations and scalable processes for producing sulfidic solid-state batteries. *Batteries Supercaps* **5**, e202200328 (2022).
30. Frith, J. T., Lacey, M. J. & Ulissi, U. A non-academic perspective on the future of lithium-based batteries. *Nat. Commun.* **14**, 420 (2023).
31. Huang, K. J., Ceder, G. & Olivetti, E. A. Manufacturing scalability implications of materials choice in inorganic solid-state batteries. *Joule* **5**, 564–580 (2021).
32. Singer, C., Schnell, J. & Reinhart, G. Scalable processing routes for the production of all-solid-state batteries—modeling interdependencies of product and process. *Energy Technol.* **9**, 2000665 (2021).

33. Dixit, M. et al. The role of isostatic pressing in large-scale production of solid-state batteries. *ACS Energy Lett.* **7**, 3936–3946 (2022).
34. Jung, K.-N., Shin, H.-S., Park, M.-S. & Lee, J.-W. Solid-state lithium batteries: bipolar design, fabrication, and electrochemistry. *ChemElectroChem* **6**, 3842–3859 (2019).
35. Famprikis, T., Canepa, P., Dawson, J. A., Islam, M. S. & Masquelier, C. Fundamentals of inorganic solid-state electrolytes for batteries. *Nat. Mater.* **18**, 1278–1291 (2019).
36. Sotoudeh, M. et al. Ion mobility in crystalline battery materials. *Adv. Energy Mater.* **14**, 2302550 (2024).
37. López, C., Emperador, A., Saucedo, E., Rurali, R. & Cazorla, C. Universal ion-transport descriptors and classes of inorganic solid-state electrolytes. *Mater. Horiz.* **10**, 1757–1768 (2023).
38. Tomkowicz, Z. & Szytuła, A. Crystal and magnetic structure of KFeO2. *J. Phys. Chem. Solids* **38**, 1117–1123 (1977).
39. Eremin, R. A., Kabanova, N. A., Morkhova, Y. A., Golov, A. A. & Blatov, V. A. High-throughput search for potential potassium ion conductors: a combination of geometrical-topological and density functional theory approaches. *Solid State Ion.* **326**, 188–199 (2018).
40. Xiao, R., Li, H. & Chen, L. High-throughput computational discovery of K 2 CdO 2 as an ion conductor for solid-state potassium-ion batteries. *J. Mater. Chem. A* **8**, 5157–5162 (2020).
41. Kato, Y. et al. High-power all-solid-state batteries using sulfide superionic conductors. *Nat. Energy* **1**, 16030 (2016).
42. Hayashi, A. et al. A sodium-ion sulfide solid electrolyte with unprecedented conductivity at room temperature. *Nat. Commun.* **10**, 5266 (2019).
43. Zhang, X. et al. Layered Oxide Cathode for Potassium-Ion Battery: Recent Progress and Prospective. *Small* **16**, 2002700 (2020).
44. Data retrieved from the Materials Project for K2Fe4O7 (mp-1120752) from database version v2022.10.28.).
45. Albrecht, R. et al. Oxo-hydroxoferrate K2−xFe4O7−x(OH)x: hydroflux synthesis, chemical and thermal instability, crystal and magnetic structures. *ChemistryOpen* **8**, 74–83 (2019).
46. Albrecht, R. et al. Tunable potassium ion conductivity and magnetism in substituted layered ferrates. *Eur. J. Inorg. Chem.* **2021**, 364–376 (2021).
47. Data retrieved from the Materials Project for Li2Fe4O7 (mp-1120820) from database version v2022.10.28.).
48. Data retrieved from the Materials Project for Na2Fe4O7 (mp-1120771) from database version v2022.10.28.).
49. Lu, X., Bowden, M. E., Sprenkle, V. L. & Liu, J. A low cost, high energy density, and long cycle life potassium–sulfur battery for grid-scale energy storage. *Adv. Mater.* **27**, 5915–5922 (2015).
50. Sabrowsky, H. et al. Die Kristallstrukturen von α- und β-K3OCl. *Z. Für. Allg. Chem.* **622**, 153–156 (1996).
51. Studenyak, I. P. et al. Synthesis and characterization of new potassium-containing argyrodite-type compounds. *Semiconduct. Phys. Quant. Electron. Optoelectron.* **22**, 26–33 (2019).
52. Lü, X. et al. Antiperovskite Li3OCl superionic conductor films for solid-state Li-ion batteries. *Adv. Sci.* **3**, 1500359 (2016).
53. Ahiavi, E. et al. Mechanochemical synthesis and ion transport properties of Na3OX (X = Cl, Br, I and BH4) antiperovskite solid electrolytes. *J. Power Sources* **471**, 228489 (2020).
54. Yu, C., van Eijck, L., Ganapathy, S. & Wagemaker, M. Synthesis, structure and electrochemical performance of the argyrodite Li6PS5Cl solid electrolyte for Li-ion solid state batteries. *Electrochim. Acta* **215**, 93–99 (2016).
55. Studenyak, I. P. et al. Structural, electrical and optical properties of ion-conducting Na6PS5Cl, Na6PS5Br, and Na7PS6 compounds. *J. Phys. Chem. Solids* **159**, 110269 (2021).
56. Wang, Y. et al. Design principles for solid-state lithium superionic conductors. *Nat. Mater.* **14**, 1026–1031 (2015).
57. Hayashi, A., Noi, K., Tanibata, N., Nagao, M. & Tatsumisago, M. High sodium ion conductivity of glass–ceramic electrolytes with cubic Na3PS4. *J. Power Sources* **258**, 420–423 (2014).
58. Chen, Y. et al. Superionic conduction in K3SbS4 enabled by Cl-modified anion lattice. *Angew. Chem. Int. Ed.* e202408574.
59. Negi S, Carvalho A, Castro Neto AH. Theoretical study of defect-mediated ionic transport in Li, Na and K b and b'' aluminas. *Phys. Rev. B* **109**, 134105 (2024).
60. Haffner, A. et al. Polymorphism and fast potassium-ion conduction in the T5 supertetrahedral phosphidosilicate KSi2 P3. *Angew. Chem. (Int. ed. Engl.)* **60**, 13641–13646 (2021).
61. Eremin, R. A., Zolotarev, P. N., Golov, A. A., Nekrasova, N. A. & Leisegang, T. Ionic transport in doped solid electrolytes by means of DFT modeling and ML approaches: a case study of Ti-Doped KFeO2. *J. Phys. Chem. C* **123**, 29533–29542 (2019).
62. Akrouchi, A. et al. First-principles study of closo-dodecaborates M 2 B 12 H 12 (M= Li, Na, K) as solid-state electrolyte materials. *Phys. Chem. Chem. Phys.* **23**, 27014–27023 (2021).
63. Wang, M. J., Kazyak, E., Dasgupta, N. P. & Sakamoto, J. Transitioning solid-state batteries from lab to market: Linking electro-chemo-mechanics with practical considerations. *Joule* **5**, 1371–1390 (2021).
64. Popovic, J. Review—recent advances in understanding potassium metal anodes. *J. Electrochem. Soc.* **169**, 030510 (2022).
65. Zheng, J. et al. Antiperovskite K3OI for K-ion solid state electrolyte. *J. Phys. Chem. Lett.* **12**, 7120–7126 (2021).
66. Wenzel, S. et al. Interfacial reactivity benchmarking of the sodium ion conductors Na3PS4 and sodium β-alumina for protected sodium metal anodes and sodium all-solid-state batteries. *ACS Appl. Mater. Interfaces* **8**, 28216–28224 (2016).
67. Lorger, S., Usiskin, R. E. & Maier, J. Transport and Charge Carrier Chemistry in Lithium Sulfide. *Adv. Funct. Mater.* **29**, 1807688 (2019).
68. Pérez, G. E. et al. Neutron and muon characterisation techniques for battery materials. *J. Mater. Chem. A* **11**, 10493–10531 (2023).
69. Vitoux, L. et al. A cylindrical cell for operando neutron diffraction of Li-ion battery electrode materials. *Front. Energy Res.* **6**, https://doi.org/10.3389/fenrg.2018.00076 (2018).
70. Rao, R. P. et al. In situ neutron diffraction monitoring of Li7La3Zr2O12 formation: toward a rational synthesis of garnet solid electrolytes. *Chem. Mater.* **27**, 2903–2910 (2015).
71. Voronin, V. I., Shekhtman, G. S. & Blatov, V. A. The natural tiling approach to cation conductivity in KAlO2 polymorphs. *Acta Crystallogr. Sect. B: Struct. Sci.* **68**, 356–363 (2012).
72. Andersson, M. et al. Interplay between the reorientational dynamics of the B3H8–anion and the structure in KB3H8. *J. Phys. Chem. C* **125**, 3716–3724 (2021).
73. Dimitrievska, M. et al. Structural and dynamical properties of potassium dodecahydro-monocarba-closo-dodecaborate: KCB11H12. *J. Phys. Chem. C* **124**, 17992–18002 (2020).
74. Gaberšček, M. Understanding Li-based battery materials via electrochemical impedance spectroscopy. *Nat. Commun.* **12**, 6513 (2021).
75. Vadhva, P. et al. Electrochemical impedance spectroscopy for all-solid-state batteries: theory, methods and future outlook. *ChemElectroChem* **8**, 1930–1947 (2021).
76. Lim, K., Fenk, B., Popovic, J. & Maier, J. Porosity of solid electrolyte interphases on alkali metal electrodes with liquid electrolytes. *ACS Appl. Mater. Interfaces* **13**, 51767–51774 (2021).
77. Eckhardt, J. K. et al. Guidelines for impedance analysis of parent metal anodes in solid-state batteries and the role of current constriction at interface voids, heterogeneities, and SEI. *Adv. Mater. Interfaces* **10**, 2202354 (2023).
78. Sedlmeier, C., Schuster, R., Schramm, C. & Gasteiger, H. A. A micro-reference electrode for electrode-resolved impedance and potential measurements in all-solid-state battery pouch cells and its application to the study of indium-lithium anodes. *J. Electrochem. Soc.* **170**, 030536 (2023).
79. Hertle, J. et al. Miniaturization of reference electrodes for solid-state lithium-ion batteries. *J. Electrochem. Soc.* **170**, 040519 (2023).

80. Liang, Z., Xiang, Y., Wang, D., Fu, R. & Yang, Y. NMR Studies of oxide-type solid state electrolytes in all solid state batteries. In: *NMR and MRI of Electrochemical Energy Storage Materials and Devices* (eds Yang Y., Fu R., Huo H.). The Royal Society of Chemistry (2021).
81. Moudrakovski, I. L. & Ripmeester, J. A. 39K NMR of solid potassium salts at 21 T: effect of quadrupolar and chemical shift tensors. *J. Phys. Chem. B* **111**, 491–495 (2007).
82. Kubicki, D. J. et al. Phase segregation in potassium-doped lead halide perovskites from 39K solid-state NMR at 21.1 T. *J. Am. Chem. Soc.* **140**, 7232–7238 (2018).
83. Wong, A., Whitehead, R. D., Gan, Z. & Wu, G. A solid-state NMR and computational study of sodium and potassium tetraphenylborates: 23Na and 39K NMR signatures for systems containing cation−π interactions. *J. Phys. Chem. A* **108**, 10551–10559 (2004).
84. Lee, P. K. et al. K-39 quadrupolar and chemical shift tensors for organic potassium complexes and diatomic molecules. *J. Phys. Chem. A* **111**, 12859–12863 (2007).
85. Michaelis, V. K., Aguiar, P. M. & Kroeker, S. Probing alkali coordination environments in alkali borate glasses by multinuclear magnetic resonance. *J. Non-Crystalline Solids* **353**, 2582–2590 (2007).
86. Glockzin, B. et al. Alkali tin halides: exploring the local structure of A2SnX6 (A = K, Rb; X = Cl, Br, I) compounds using solid-state NMR and DFT computations. *J. Phys. Chem. C* **127**, 7284–7298 (2023).
87. Wang, W., Wang, Y., Wang, C.-H., Yang, Y.-W. & Lu, Y.-C. In Situ probing of solid/liquid interfaces of potassium–oxygen batteries via ambient pressure X-ray photoelectron spectroscopy: new reaction pathways and root cause of battery degradation. *Energy Storage Mater.* **36**, 341–346 (2021).
88. Caracciolo, L., Madec, L. & Martinez, H. XPS analysis of K-based reference compounds to allow reliable studies of solid electrolyte interphase in K-ion batteries. *ACS Appl. Energy Mater.* **4**, 11693–11699 (2021).
89. Deng, Z. et al. Towards autonomous high-throughput multiscale modelling of battery interfaces. *Energy Environ. Sci.* **15**, 579–594 (2022).
90. Shao, J. et al. K 3 SbS 4 as a potassium superionic conductor with low activation energy for K–S batteries. *Angew. Chem.* **134**, https://doi.org/10.1002/ange.202200606 (2022).
91. Yuan, H. et al. A K 2 Fe 4 O 7 superionic conductor for all-solid-state potassium metal batteries. *J. Mater. Chem. A* **6**, 8413–8418 (2018).
92. Whittingham, M. Proceedings of the 5th material research symposium. *Solid State Chem.* **364**, 139–154 (1972).
93. Burmakin, E., Antonov, B. & Shekhtman, G. S. Potassium ion conducting K 1− 2 x Cd x FeO 2 solid electrolytes. *Inorg. Mater.* **46**, 540–544 (2010).
94. Burmakin, E. & Nechaev, G. Solid potassium-conducting electrolytes in the K 2− 2 x Ga 2− x V x O 4 system. *Russian J. Electrochem.* **49**, 1001–1003 (2013).
95. Burmakin, E., Nechaev, G. & Shekhtman, G. S. Solid electrolytes with potassium cation conductivity in K 1− 2 x M x AlO 2 (M= Ba, Pb) systems. *Russian J. Electrochem.* **44**, 1386–1392 (2008).
96. Burmakin, E. & Shekhtman, G. S. Potassium ion conducting K 2− 2 x Fe 2− x P x O 4 solid electrolytes. *Inorg. Mater.* **44**, 882–885 (2008).
97. Nechaev, G. & Burmakin, E. Potassium-conducting solid electrolytes in K 1− 2 x Sr x GaO 2 system. *Russian J. Electrochem.* **47**, 1411–1414 (2011).
98. Nechaev, G., Burmakin, E. & Potassium–conducting, K. 1− 2 x Pb x GaO 2 solid electrolytes. *Russian J. Electrochem.* **47**, 457–460 (2011).
99. Doux, J.-M. et al. New KRb 2 Sb 4 BO 13 and Rb 3 Sb 4 BO 13 compounds prepared by Rb+/K+ ion exchange from the K 3 Sb 4 BO 13 ion conductor. *CrystEngComm* **21**, 594–601 (2019).
100. Wang, E. & Greenblatt, M. Ionic conductivity of potassium phosphatoantimonates and some of their ion-exchanged analogs. *Chem. Mater.* **3**, 542–546 (1991).
101. Burmakin, E., Voronin, V., Akhtyamova, L., Berger, I. & Shekhtman, G. S. Solid electrolytes based on KAlO 2-TiO 2: the crystalline structure and conduction. *Russian J. Electrochem.* **41**, 783–788 (2005).
102. Takahashi, T. & Kuwabara, K. Ionic conductivities of hollandites. *Electrochim. Acta* **23**, 375–379 (1978).
103. Zhang, Y. et al. KB3H8· NH3B3H7 complex as a potential solid-state electrolyte with excellent stability against K metal. *ACS Appl. Mater. Interfaces* **14**, 17378–17387 (2022).
104. Wang, J., Lei, G., He, T., Cao, H. & Chen, P. Defect-rich potassium amide: a new solid-state potassium ion electrolyte. *J. Energy Chem.* **69**, 555–560 (2022).
105. Spencer Jolly, D. et al. High critical currents for dendrite penetration and voiding in potassium metal anode solid-state batteries. *J. Solid State Electrochem.* **26**, 1961–1968 (2022).
106. Quérel, E., Williams, N. J., Seymour, I. D., Skinner, S. J. & Aguadero, A. Operando characterization and theoretical modeling of metal| electrolyte interphase growth kinetics in solid-state batteries. Part I: experiments. *Chem. Mater.* **35**, 853–862 (2023).

Author contributions

J.G. and J.P.-N. conceived the project. S.K.S. and I.E.C. lead the writing of the manuscript sections dealing with materials modeling. D.L. Q.C. lead the writing of the manuscript sections dealing with neutron-based characterization techniques. J.G. and J.P.-N. lead the writing of all other manuscript sections, coordinated, and edited the manuscript prior to submission and in the revision phase.

Competing interests

The authors declare no competing interests.

Additional information

Supplementary information The online version contains supplementary material available at https://doi.org/10.1038/s43246-024-00568-3.

Correspondence and requests for materials should be addressed to Jelena Popovic-Neuber.

Peer review information *Communications Materials* thanks nobuto yoshinari and the other, anonymous, reviewer(s) for their contribution to the peer review of this work. Primary Handling Editors: Saneyuki Ohno and Jet-Sing Lee.